PCCP

PAPER

View Article Online
View Journal | View Issue

Cite this: *Phys. Chem. Chem. Phys.*, 2019, **21**, 148

Carbon chain growth by formyl coupling over the Cu/γ-AlOOH(001) surface in syngas conversion†

Hui Bai, *[ab] Mengmeng Ma,[a] Bing Bai,[ab] Haojie Cao,[a] Lin Zhang,[a] Zhihua Gao,[a] Vladimir A. Vinokurov[c] and Wei Huang *[a]

Catalytic conversion of syngas to valuable chemicals and fuels such as ethanol is an extremely desirable process route. In the present study, the elementary steps leading to the formation of ethanol *via* syngas conversion over the Cu/γ-AlOOH(001) surface have been explored using density functional theory (DFT) calculations. The reaction pathway CO + H → CHO, CHO + CHO → OHCCHO → CHCHO + O, CHCHO + 4H → CH_2CHO + 3H → CH_3CHO + 2H → CH_3CH_2O + H → C_2H_5OH is the most favorable; during the whole process, CH_3CHO formation needs to overcome the highest activation barrier. Different from the γ-AlOOH(001) surface, carbon chain growth is realized *via* the formyl coupling mechanism on the Cu/γ-AlOOH(001) surface; this step needs to overcome a 1.07 eV activation barrier and is exothermic by 0.73 eV. Our Bader charge analyses revealed that the addition of the Cu component enhances the electrostatic interaction between the CHO intermediate and the γ-AlOOH(001) surface with the aid of the formed CuO_x species; as a result, the initial C–C chain forms in a different way. Moreover, the rate constant results manifest that the formation of the OHCCHO key intermediate can be facilitated by increasing the reaction temperature. We expect the obtained results will be useful for future experimental studies to improve the selectivity of C_2 oxygenates in syngas conversion.

Received 22nd October 2018,
Accepted 16th November 2018

DOI: 10.1039/c8cp06582a

rsc.li/pccp

1 Introduction

As the key bridge between various carbon resources (including coal, natural gas and biomass) and liquid fuels or high-value chemicals, syngas (CO/H_2) has attracted much attention due to the increasing demand for energy and the limited availability of easily accessible petroleum resources.[1–3] Syngas can be selectively converted to alcohols, aldehydes, and carboxylic acids. With respect to the energy sector, ethanol is a more suitable product because it can serve as a clean fuel, an additive for gasoline to increase the octane number and the combustion efficiency in automobiles,[4,5] and feedstock for the synthesis of a variety of chemicals, fuels, and polymers.[6,7] Moreover, ethanol possesses potential as an alternative hydrogen carrier to the more toxic and less energy-dense methanol in fuel cell technologies.[8–10] Therefore, the direct conversion of syngas to ethanol is an extremely desirable process.[11,12] This field of research has focused mainly on the development of a catalyst with acceptable activity and selectivity toward ethanol. However, low yield and poor selectivity for ethanol formation from syngas remain the major hurdles associated with the use of known catalysts.[13]

The process of ethanol synthesis from syngas generally involves several key steps, including initial CO activation, C_1–C_2 linear chain growth, and successive hydrogenation to ethanol.[14–16] Among the existing conventional catalysts for ethanol synthesis, Cu-based catalysts are typical modified methanol synthesis catalysts that are regarded as an attractive option due to their low price, mild reaction conditions and desirable capability to catalyze hydrogenation reactions. However, due to their insufficient ethanol yields, these catalysts are unattractive for commercial applications.[13,14,17] Especially, compared with alkali-modified CuCo-based FT catalysts and MoS_2-based catalysts, alkali-modified Cu–ZnO/Al_2O_3 catalysts shows the lowest ethanol yield but exhibits higher selectivity toward ethanol than hydrocarbons.[13] Subsequently, a large number of studies on modified Cu-based methanol catalysts for syngas conversion to ethanol have been reported.[12,13,18–20] Alkali-modified Cu/Zn and Cu/Zn/Al systems have been extensively studied.[12] It is noteworthy that our previous

[a] *Key Laboratory of Coal Science and Technology of Ministry of Education and Shanxi Province, Taiyuan University of Technology, Taiyuan 030024, China. E-mail: baihui@tyut.edu.cn, huangwei@tyut.edu.cn*
[b] *Department of Chemistry, Brown University, Providence, RI 02912, USA*
[c] *Department of Physical and Colloid Chemistry, Gubkin Russian State University of Oil and Gas (National Research University), Leninskiy prospect 65/1, Moscow, 119991, Russia*

† Electronic supplementary information (ESI) available: The most stable adsorption configurations of possible species involved in the pathways of syngas-to-ethanol conversion over Cu/γ-AlOOH(001) surface; the potential energy profile for OHCCHO hydrogenation with the structures of initial states (ISs), transition states (TSs), and final states (FSs); the potential energy profile for OH_2CCHO hydrogenation with the structures of initial states (ISs), transition states (TSs), and final states (FSs); and the potential energy profile for (a) HOH_2CCHO hydrogenation and (b) HOH_2CCH_2OH formation with the structures of initial states (ISs), transition states (TSs), and final states (FSs). See DOI: 10.1039/c8cp06582a

experimental results found that a CuZnAl catalyst without promoters, which is prepared by complete liquid-phase technology, could directly synthesize ethanol from syngas.[21–23] Moreover, it has been identified that the Al species is generally formed as γ-AlOOH phase, and it has been suggested that γ-AlOOH has the function of CO activation and chain growth, which favor the formation of higher alcohols.[24–27] Intriguingly, our previous experimental work[28,29] showed that AlOOH has an obvious influence on the distribution of products of CO hydrogenation and shows excellent selectivity for acetaldehyde in the reaction of methanol and syngas. Therefore, we deem that γ-AlOOH not only serves as the catalyst support but also exhibits good catalytic activities for syngas conversion. Furthermore, our recent theoretical results have verified that both γ-AlOOH(100)[30] and γ-AlOOH(001)[31] surfaces, which are among the primary exposed surfaces of γ-AlOOH crystal,[32–35] show particular reactivity for C–C chain formation during the process of ethanol synthesis. Furthermore, the γ-AlOOH(001) surface displays better catalytic activity for formation of the key species CH_x.[31] Actually, the nature of the catalyst support has an important influence on the stability and growth of the active components[36] and also on the reactions taking place over the catalysts.[37–39] Thus, it can be readily assumed that under realistic reaction conditions of syngas-to-ethanol conversion over the Cu-based catalyst, if the catalyst-support interaction alters the pathway and ultimately affects the selectivity of syngas conversion. Therefore, making efforts is required to elucidate the effects of the interaction between the Cu and Al components in CuZnAl catalysts during ethanol synthesis for better understanding the reaction mechanism.

Based on our previous research,[30,31] the present study aims to elucidate the reaction mechanism of ethanol formation from syngas over the Cu/γ-AlOOH(001) surface using DFT calculations. The important elementary reactions for ethanol synthesis, including the hydrogenation of CO to CHO, CHO coupling to realize C–C chain growth and hydrogenation of C_2 oxygenates to ethanol, are examined. These elementary steps are crucial for the reaction mechanism and the overall reactivity of ethanol synthesis. Eventually, a clear picture of ethanol formation from syngas over the Cu/γ-AlOOH(001) surface was obtained and was then compared with our recent results on a γ-AlOOH(001) surface.[31] To gain more precise insights into the initial formation of the C–C chain, the charge distributions of the Cu/γ-AlOOH(001) surface and relative adsorbed intermediates have been studied by Bader charge analysis. Meanwhile, considering the effects of temperature on ethanol formation, the rate constants of some key elementary reactions along the optimal pathway in the range of 543 to 583 K were calculated. The detailed characterization of syngas conversion into ethanol over the Cu/γ-AlOOH(001) surface at the molecular level will aid understanding of the underlying reaction mechanisms and further provide new ideas for designing better, more stable catalysts with higher reactivity.

2 Computational details

To date, a great deal of effort has been devoted to determine the catalytic mechanism of syngas conversion on the Cu-based catalysts. Recently reported results[40] revealed that a smaller Cu cluster size corresponds to higher selectivity of C_2 oxygenates. Combining the characteristics of Cu clusters and the simplicity of calculation, a Cu_4 cluster, which is the smallest unit that presents a three-dimensional structure, was adopted to represent the Cu component in the Cu/γ-AlOOH catalyst. On the other hand, considering the specific surface area, coordination environment, and surface stability of γ-AlOOH crystal,[41,42] for comparison with our previous study on the mechanism of ethanol synthesis from syngas on a γ-AlOOH(001) surface[31] and to ascertain the interaction between the Cu and Al components, the γ-AlOOH(001) surface was chosen to represent the Al component in the Cu/γ-AlOOH catalyst. The γ-AlOOH(001) surface was modeled by a six-layer slab and periodically repeated in a (4 × 1) lateral supercell. Furthermore, a 15 Å vacuum gap perpendicular to the surface was employed to prevent interactions between any two successive slabs. As shown in Fig. 1, the Cu_4 cluster with a 3D tetrahedral configuration adsorbed on the γ-AlOOH(001) surface was selected as the Cu/γ-AlOOH model catalyst, in which the Cu_4 cluster bonds with three O sites on the γ-AlOOH(001) surface. Here, the partial coverage of CuO_x species was formed by strong metal support interactions (SMSI) between the Cu component and the γ-AlOOH(001) surface. Moreover, six different adsorption sites on the surface were considered; these were labeled as Cu_1, Cu_2, Cu_3, Cu_4, Al_V and O_3, respectively. In all calculations, the bottom two layers of γ-AlOOH(001) were fixed, while the other four layers and the Cu_4 cluster were allowed to relax.

In this work, the Vienna *ab initio* Simulation Package (VASP)[43,44] was used to perform all DFT computations. The exchange–correlation energies were calculated using the Perdew–Burke–Ernzerhof functional (PBE) within the generalized gradient approximation (GGA).[45] The projector-augmented wave (PAW) method[46,47] was employed to express the electron–ion interactions, and the electronic wave function was considered by setting the plane-wave energy cutoff at 400 eV. The dispersion-corrected DFT (DFT-dDsC) scheme was used to describe the van der Waals (vdW) interactions.[48,49] In addition, the maximum force on the atoms was converged to less than 0.03 eV $Å^{-1}$ and the Brillouin zone was sampled by the 3 × 3 × 1 grid Monkhorst–Pack special *k*-point in all calculations.[50] The isolated atoms and molecules were calculated in a 10 × 10 × 10 $Å^3$ cubic unit cell. Frequency analysis was used to validate the optimized transition state structures with only one imaginary frequency.[51]

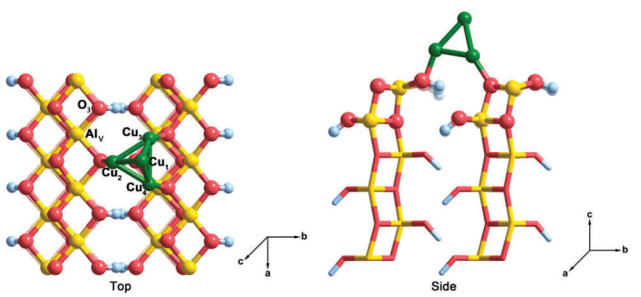

Fig. 1 Top and side views of the Cu/γ-AlOOH(001) surface. Green spheres represent Cu atoms, gold spheres represent Al atoms, pink spheres represent O atoms and pale blue spheres represent H atoms.

The adsorption energies (E_{ads}) of all species were obtained using the following equation:

$$E_{ads} = [E_{adsorbate} + E_{slab}] - E_{adsorbate/slab}$$

where $E_{adsorbate}$, E_{slab}, and $E_{adsorbate/slab}$ refer to the total energies of the free adsorbate, the clean Cu/γ-AlOOH(001) surface slab, and the slab with the adsorbate, respectively. The reaction energy (ΔE) and activation barrier (E_a) were calculated as:

$$\Delta E = E_{FS} - E_{IS}$$

$$E_a = E_{TS} - E_{IS}$$

where E_{IS}, E_{TS} and E_{FS} correspond to the total energies of the initial state (IS), transition state (TS), and final state (FS), respectively.

In view of the influences of the zero-point vibrational energy (ZPE), thermal energy and entropy on the standard molar Gibbs free energies, thermodynamic statistical formulas rooted in partition functions were employed to correct the energies obtained directly from DFT calculations. The standard molar Gibbs free energy can be acquired from the following equation:[52]

$$G^{\theta}(T,p) = E_{total} + E_{ZPE} + U^{\theta} - TS^{\theta} + \gamma RT[1 + \ln(p/p^{\theta})]$$

where E_{total} represents the total energy of the DFT calculations, E_{ZPE} is the zero-point vibrational energy, and U^{θ} and S^{θ} are the thermal energy and entropy, respectively. γ is 0 for surface-adsorbed species and 1 for gaseous molecules, R is the gas constant, and p is the partial pressure of the gas-phase molecule. Our previous studies examined the product distribution of the syngas conversion; we found that the selectivity of ethanol can reach 27.4% at 563 K.[53] As listed in Table 3, the temperature of 563 K was chosen in the equations of the activation barrier (ΔG_a) and reaction energy (ΔG). By comparing these values with E_a and ΔE, we can determine whether it is feasible to explore the optimal reaction pathway ethanol synthesis from syngas based on these values.

To consider the effects of the temperature of ethanol synthesis over the Cu/γ-AlOOH(001) surface, the rate constants at different reaction temperatures were calculated by employing Transition State Theory (TST).[54,55]

The corresponding equation[56,57] can be described as follows:

$$k = A\exp\left(-\frac{E_a}{RT}\right) = \frac{k_B T}{h}\frac{Q_{TS}}{Q_R}\exp\left(-\frac{E_a}{RT}\right)$$

where A, E_a, T, k_B, and h are the prefactor, activation energy, reaction temperature, Boltzmann constant and Planck constant, respectively. Q_{TS} and Q_R are the partition functions per unit volume for a TS and a reactant, respectively. The partition function per unit volume (Q), which is related to statistical thermodynamics, can be estimated by vibrational partition functions as follows:

$$Q^{vib} = \prod_i \frac{\exp(-hv_i/2k_BT)}{1-\exp(-hv_i/k_BT)}$$

where v_i is the frequency of vibrational mode i. Therefore, the prefactors[58] can be calculated as follows:

$$A = \frac{k_B T}{h}\frac{Q_{TS}^{vib}}{Q_R^{vib}}$$

3 Results and discussion

3.1 Adsorption of all possible species

In order to investigate the formation mechanism of ethanol, the geometry structures and energy characteristics of all possible species involved in ethanol synthesis were examined in detail. The most stable adsorption configurations are displayed in Fig. S1 (ESI†), and the corresponding adsorption energies and key geometrical parameters are listed in Table 1.

3.1.1 C, O, CO, CO_2, H, OH, H_2, CH_x (x = 1, 2), COH, CH_xO (x = 1, 2), CHOH. As the initial reactants, CO and H can be widely adsorbed over the Cu/γ-AlOOH(001) surface. In this section, all possible adsorption sites of CO and H are considered. Our results show that CO prefers to bond with the Cu_2 site through the C atom, and H is adsorbed at the bridge Cu_2–Cu_3 site; the corresponding adsorption energies are 1.37 and 3.86 eV, respectively. C and CH prefer to bond with the Cu_1, Cu_2, Cu_3 and Cu_4 sites *via* C atoms, and the adsorption energies are 7.23 and 6.83 eV, respectively. O and OH prefer to adsorb at the three-fold hollow Cu_1–Cu_2–Cu_3 and bridge Cu_1–Cu_2 sites with the corresponding adsorption energies of 7.24 and 4.84 eV, respectively.

Table 1 Adsorption energies (eV) and key geometrical parameters (Å) of possible species involved in syngas conversion over the Cu/γ-AlOOH(001) surface

Species	E_{ads}	Configuration	Key parameters
C	7.23	Cu_1, Cu_2, Cu_3 and Cu_4	Cu_1–C: 1.822 Cu_2–C: 1.851 Cu_3–C: 1.838 Cu_4–C: 1.881
H	3.86	Cu_2 and Cu_3	Cu_2–H: 1.687 Cu_3–H: 1.554
O	7.24	Cu_1, Cu_3 and Cu_4	Cu_1–O: 1.846 Cu_3–O: 1.870 Cu_4–O: 1.863
OH	4.84	Cu_2 and Cu_3	Cu_2–O: 1.924 Cu_3–O: 1.873
CO	1.37	Cu_2	Cu_2–C: 1.825
CH	6.83	Cu_1, Cu_2, Cu_3 and Cu_4	Cu_1–C: 1.944 Cu_2–C: 1.886 Cu_3–C: 1.932 Cu_4–C: 1.966
CH_2	4.72	Cu_1, Cu_2 and Cu_4	Cu_1–C: 1.981 Cu_3–C: 1.918 Cu_4–C: 2.014
COH	3.87	Cu_1, Cu_2 and Cu_4	Cu_1–C: 1.957 Cu_3–C: 1.861 Cu_4–C: 1.860
CHO	2.66	Cu_1 and Cu_2	Cu_1–O: 2.047 Cu_2–C: 1.888
CHOH	2.50	Cu_1 and Cu_2	Cu_1–O: 2.065 Cu_2–C: 1.868
CH_2O	0.86	Cu_1 and Cu_2	Cu_1–O: 1.926 Cu_2–C: 2.204
OCCHO	1.71	Cu_1, Cu_2 and Cu_3	Cu_1–O_1: 1.965 Cu_2–C_1: 2.262 Cu_3–O_1: 2.011
OHCCHO	2.13	Cu_1 and Cu_3	Cu_1–O_1: 1.907 Cu_3–O_2: 1.851
CHCHO	4.71	Cu_1, Cu_2 and Cu_3	Cu_1–O: 1.946 Cu_2–C_2: 1.955 Cu_3–C_2: 1.942
CHCHOH	3.61	Cu_1 and Cu_2	Cu_1–O: 2.064 Cu_2–C_2: 1.912
CH_2CHO	3.31	Cu_1 and Cu_2	Cu_1–O: 1.958 Cu_2–C_2: 2.060
CH_2CHOH	1.14	Cu_2	Cu_2–C_1: 2.189 Cu_2–C_2: 2.104
CH_3CHO	0.99	Cu_1	Cu_1–O: 1.949
CH_3CHOH	1.00	Cu_1	Cu_1–O: 2.032
CH_3CH_2O	3.40	Cu_1	Cu_1–O: 1.812
C_2H_5OH	0.88	Cu_1	Cu_1–O: 2.034
CO_2	0.31	Upon Al_V and O_3	Al_V–O_1: 3.236 O_3–C: 2.871
H_2	0.39	Cu_2	Cu_2–H_1: 1.734 Cu_2–H_2: 1.690

CH_2 prefers to stay on the three-fold hollow Cu_1–Cu_2–Cu_4 site, with an adsorption energy of 4.72 eV. Complete geometry optimization reveals that the Cu_2 site is the most stable adsorption site for H_2 on the Cu/γ-AlOOH(001) surface; the calculated adsorption energy is 0.39 eV. The adsorption behavior of the CO_2 molecule was also considered here; it is suspended on the Al_V and O_3 sites, with an adsorption energy of 0.31 eV. According to our calculations, COH prefers to occupy the three-fold hollow Cu_1–Cu_2–Cu_4 site, with a corresponding adsorption energy of 3.87 eV. Additionally, CHO, CH_2O and CHOH adsorb favorably at the bridge Cu_1–Cu_2 site *via* both C and O atoms; their adsorption energies are 2.66, 0.86 and 2.50 eV, respectively.

3.1.2 OCCHO, OHCCHO, CH_xCHO (x = 1 to 3), CH_xCHOH (x = 1 to 3), CH_3CH_2O, C_2H_5OH. As an important intermediate in the synthesis of ethanol from syngas over the Cu/γ-AlOOH(001) surface, OHCCHO prefers to sit at the bridge Cu_1–Cu_3 site through two O atoms with a corresponding adsorption energy of 2.13 eV. Our calculation suggests that CH_2CHOH can be located at the Cu_2 site on the Cu/γ-AlOOH(001) surface, stabilizing the system by an adsorption energy of 1.14 eV. Similar to the most stable adsorption configuration of OHCCHO, CHCHOH and CH_2CHO can remain stable on the Cu_1–Cu_2 site; their adsorption energies are 3.61 and 3.31 eV, respectively. It has been verified that the most stable adsorption sites of OCCHO and CHCHO are the three-fold hollow Cu_1–Cu_2–Cu_3 site, with corresponding adsorption energies of 1.71 and 4.71 eV, respectively. Geometry optimization reveals that the Cu_1 site is the most stable adsorption site for CH_3CHO, CH_3CHOH, CH_3CH_2O and C_2H_5OH; the calculated adsorption energies are 0.99, 1.00, 3.40 and 0.88 eV, respectively.

Based on the above results, we can conclude that most species prefer to interact with the Cu_4 cluster on the γ-AlOOH(001) surface. Compared with our previously reported γ-AlOOH(001) surface,[31] the adsorption abilities of the C, H, CH_2, COH, CHO, CHOH, CH_2O, OCCHO, CHCHO, CHCHOH and CH_2CHOH species involved in ethanol synthesis on the Cu/γ-AlOOH(001) surface decrease to a variable extent. However, the adsorption energies of the O, OH, H_2, CO, CO_2, CH, OHCCHO and C_2H_5OH species increase to some extent. Regardless, the adsorption abilities of most common species on the Cu/γ-AlOOH(001) surface are stronger than those on the Cu(211) surface.[14]

3.2 The key steps of ethanol formation

As listed in Table 2, the activation barriers (E_a), reaction energies (ΔE) and key geometrical parameters of the possible elementary steps during the process of ethanol synthesis were considered. Potential energy profiles for the possible reaction pathways are discussed and depicted in Fig. 2–7. Based on the above investigations, an optimal reaction pathway was identified by comparing the corresponding activation barriers and reaction energies. In addition, frequency analysis was used to validate the optimized transition state structure. In this section, we divide the reaction process into three parts: CO initial activation, C–C chain growth and C_2H_5OH formation, concretely including the hydrogenation of CO to CHO, CHO coupling to realize C–C chain growth and the hydrogenation of C_2 oxygenates to ethanol.

3.2.1 Initial CO activation. As the initial key step for ethanol formation, initial CO activation is generally considered to have three possibilities: direct dissociation of CO, hydrogenation of CO to COH, and hydrogenation of CO to CHO. Our calculation results show that the direct dissociation of CO is impossible because of its high reaction energy of 3.71 eV on the Cu/γ-AlOOH(001) surface. Therefore, two possible products remain for initial CO activation: COH and CHO.

Starting with the co-adsorbed CO and H, in which CO adsorbs at the Cu_2 site *via* the C atom and H remains at the bridge of the Cu_2–Cu_4 site, the distance between the O and H atoms decreases to 1.243 Å in TS1 from 4.057 Å in the initial state during the formation of COH. As shown in Fig. 2, the adsorbed CO molecule moves to the three-fold hollow Cu_1–Cu_2–Cu_4 site and the dissociative H atom migrates to the C–O bridge site of CO in TS1; then, the C–H bond breaks to form the COH species. This process must overcome a high activation barrier of 3.02 eV with a

Table 2 Activation barriers (eV), reaction energies (eV) and key geometrical parameters (Å) of the elementary steps involved in ethanol synthesis from syngas over the Cu/γ-AlOOH(001) surface

Reaction		E_a	ΔE	ISs key parameter	TSs key parameter	ν
(R1)	CO + H → COH	3.02	1.29	O–H: 4.057	O–H: 1.243	1723i
(R2)	CO + H → CHO	1.30	0.55	C–H: 3.017	C–H: 1.475	511i
(R3)	CHO + H → CH + OH	3.00	−0.10	C–O: 1.278 O–H: 3.416	C–O: 2.559 O–H: 2.568	105i
(R4)	CHO + H → CHOH	2.28	1.00	O–H: 3.416	O–H: 2.215	576i
(R5)	CHO + H → CH_2O	1.94	0.33	C–H: 3.655	C–H: 1.899	530i
(R6)	CHO + H → CH_2 + O	1.47	0.52	C–H: 3.655 C–O: 1.278	C–H: 1.914 C–O: 1.409	29i
(R7)	CHO + CO → CH + CO_2	1.42	0.05	C_2–O_1: 3.454	C_2–O_1: 1.366	149i
(R8)	CHO + CO → OCCHO	1.22	0.98	C_1–C_2: 3.956	C_1–C_2: 2.357	151i
(R9)	CHO + CHO → OHCCHO	1.07	−0.73	C_1–C_2: 4.177	C_1–C_2: 2.412	349i
(R10)	OHCCHO → CHCHO + O	1.51	0.34	C_2–O_2: 1.318	C_2–O_2: 2.689	219i
(R11)	CHCHO + H → CHCHOH	2.82	1.73	O–H: 4.461	O–H: 2.450	77i
(R12)	CHCHO + H → CH_2CHO	1.09	−0.95	C_2–H: 4.071	C_2–H: 2.076	95i
(R13)	CH_2CHO + H → CH_2CHOH	1.77	0.56	O–H: 3.223	O–H: 1.840	469i
(R14)	CH_2CHO + H → CH_3CHO	1.58	0.52	C_2–H: 3.786	C_2–H: 2.536	218i
(R15)	CH_3CHO + H → CH_3CHOH	1.67	1.55	O–H: 2.952	O–H: 1.708	94i
(R16)	CH_3CHO + H → CH_3CH_2O	1.01	−0.38	C_1–H: 3.641	C_1–H: 2.559	498i
(R17)	CH_3CH_2O + H → C_2H_5OH	1.35	−0.13	C_1–H: 3.319	C_1–H: 1.730	851i

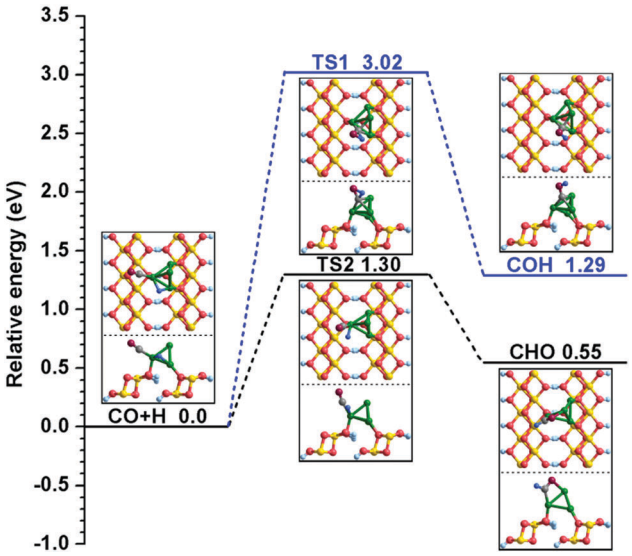

Fig. 2 The potential energy profile for initial CO activation with the structures of the initial states (ISs), transition states (TSs), and final states (FSs). Green spheres represent Cu atoms, gold spheres represent Al atoms, pink spheres represent O atoms, pale blue spheres represent H atoms and gray spheres represent C atoms. To distinguish the O and H atoms of the Cu/γ-AlOOH(001) surface from the O and H atoms of the adsorbates, the O and H atoms of the adsorbates are displayed as brown and light blue spheres, respectively.

reaction energy of 1.29 eV. On the other hand, for CHO formation, the distance between the C and H atoms decreases to 1.475 Å in TS2 from 3.017 Å in the initial state. In TS2, the O atom of the CO molecule gradually approaches the Cu_1 site; meanwhile, the H atom moves to the Cu_2 site. After TS2, the H atom bonds with the C atom to form the key intermediate CHO. The calculated activation barrier and reaction energy are 1.30 and 0.55 eV, respectively. By comparing the calculation results of (R1) and (R2), we obtain the information that the CO + H → CHO reaction is more favorable both kinetically and thermodynamically on the Cu/γ-AlOOH(001) surface, which is consistent with γ-AlOOH(001)[31] and Cu(211)[14] surfaces. The CHO species is a key intermediate in many reactions[59,60] with respect to syngas conversion to ethanol.

3.2.2 C–C chain growth. It has been confirmed that the initial C–C chain formation is the rate-determining step for C_{2+}OH production, and subsequent chain growth is attributed to aldol condensation reactions.[61] For CuZnAl catalysts, the initial C–C bond formation is predominately attributed to the coupling of two C_1 intermediates that can be derived from syngas.[61,62] Meanwhile, significant experimental and theoretical efforts[14–16,19,63,64] have found that CH_x (x = 1 to 3) is the key intermediate in the process of ethanol synthesis from syngas on Cu-based catalysts; subsequently, CO or CHO inserts into CH_x (x = 2, 3), which leads to C_2 oxygenates. Meanwhile, on the Cu/γ-AlOOH(001) surface, our calculation results verified that

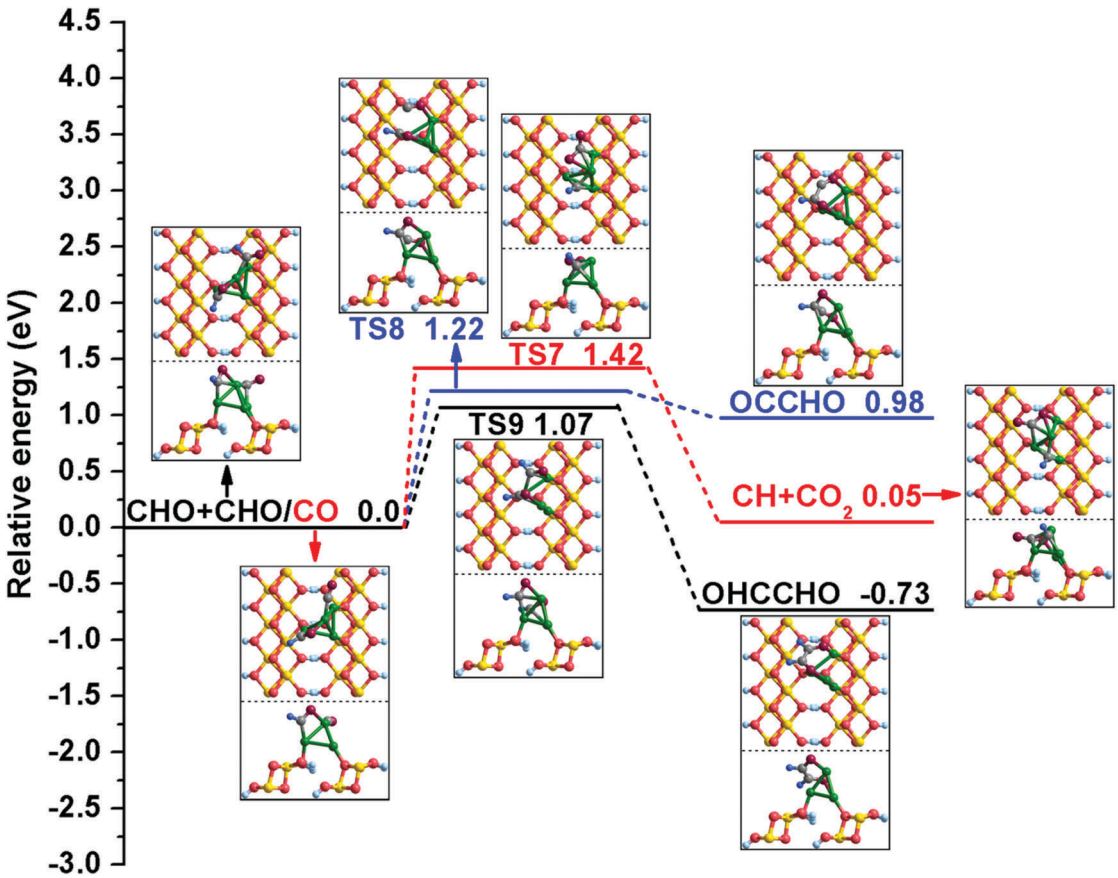

Fig. 3 The potential energy profile for initial C–C chain formation with the structures of the initial states (ISs), transition states (TSs), and final states (FSs).

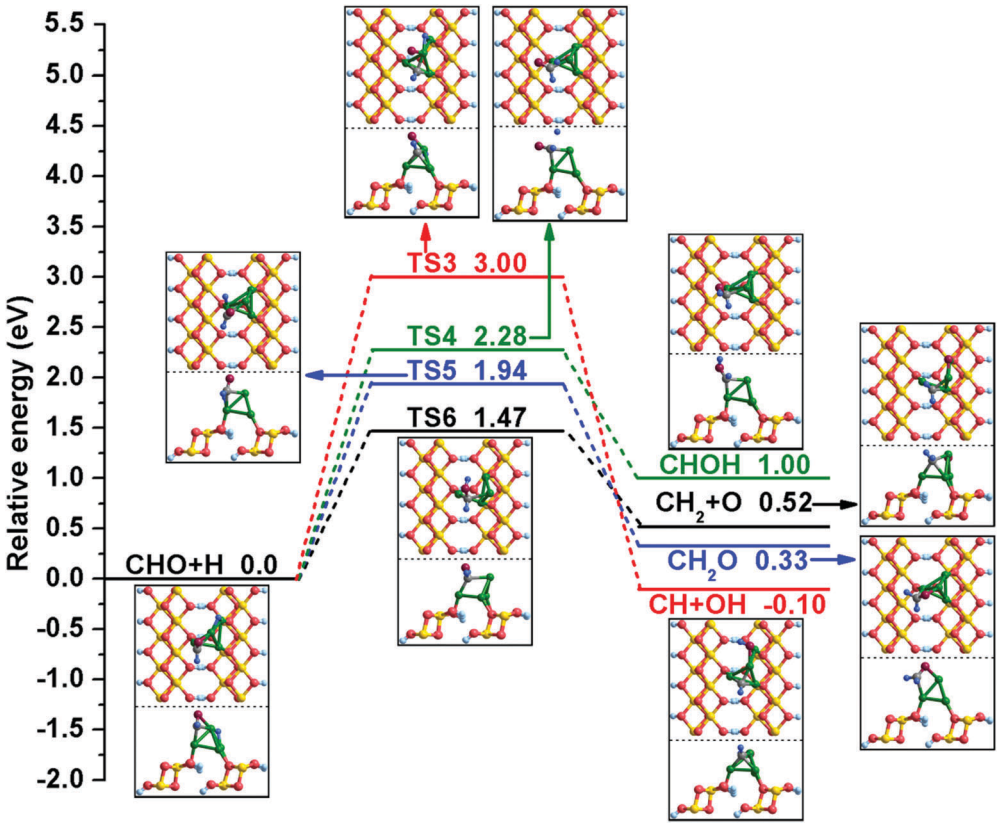

Fig. 4 The potential energy profile for CHO hydrogenation with the structures of the initial states (ISs), transition states (TSs), and final states (FSs).

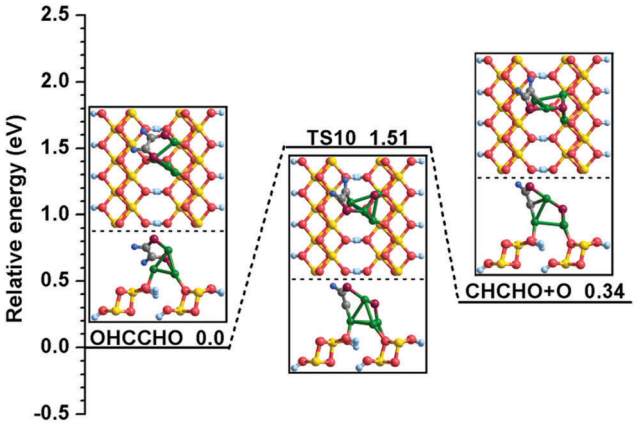

Fig. 5 The potential energy profile for C–O bond cleavage with the structures of the initial states (ISs), transition states (TSs), and final states (FSs).

the initial C–C chain formation is mainly due to the coupling of two CHO intermediates, which is the predominant cause of CO initial activation. As presented in Fig. 3, one CHO resides in the bridge Cu_1–Cu_3 site *via* the C atom and the other CHO bonds with the Cu_1 and Cu_2 sites through the C and O atoms in the initial state. Then, the two CHO move close to each other, and the distance between the two C atoms decreases to 2.412 Å in TS9 from 4.177 Å in the initial state. Finally, the C_2 species OHCCHO is formed when the two C atoms bond with each other. The co-adsorption energy of CHO + CHO is 5.26 eV, which is slightly smaller than the sum of two CHO species (2.66 + 2.66 eV) on the surface. Therefore, the interaction between co-adsorbed CHO and CHO is almost negligible. On the Cu/γ-AlOOH(001) surface, the C–C chain growth must overcome an activation barrier of 1.07 eV, accompanied by a reaction energy of −0.73 eV. Furthermore, as summarized in Table 3, our calculated activation free energy of C–C chain growth *via* CHO coupling is 1.09 eV, with a reaction free energy of −0.58 eV; this is almost in agreement with our E_a and ΔE results. The activation barrier of C–C chain growth *via* CHO coupling to form OHCCHO in (R9) is remarkably lower than a previously reported corresponding barrier *via* CO insertion into CH_3 to form CH_3CO on Cu(211),[14] but is higher than the barrier *via* CO insertion into CH to form CHCO over the γ-AlOOH(001) surface.[31] Moreover, the barrier of (R9) for carbon chain growth on the Cu/γ-AlOOH(001) surface is very similar to that on a CuZnAl catalyst (0.96 eV).[15]

Meanwhile, C–C bond formation *via* the coupling reaction between CHO and CO is also considered here. For (R8), the formation of OCCHO is endothermic by 0.98 eV, with an activation barrier of 1.22 eV. During this process, the distance between two C atoms decreases to 2.357 Å in TS8 from 3.956 Å in the co-adsorbed CHO and CO. For comparison with the γ-AlOOH(001) surface,[31] the possible elementary reaction CHO + CO → CH + CO_2 was also calculated, and the relative computation results show that the activation barrier and reaction energy of the step are 1.42 and 0.05 eV, respectively. It can be seen

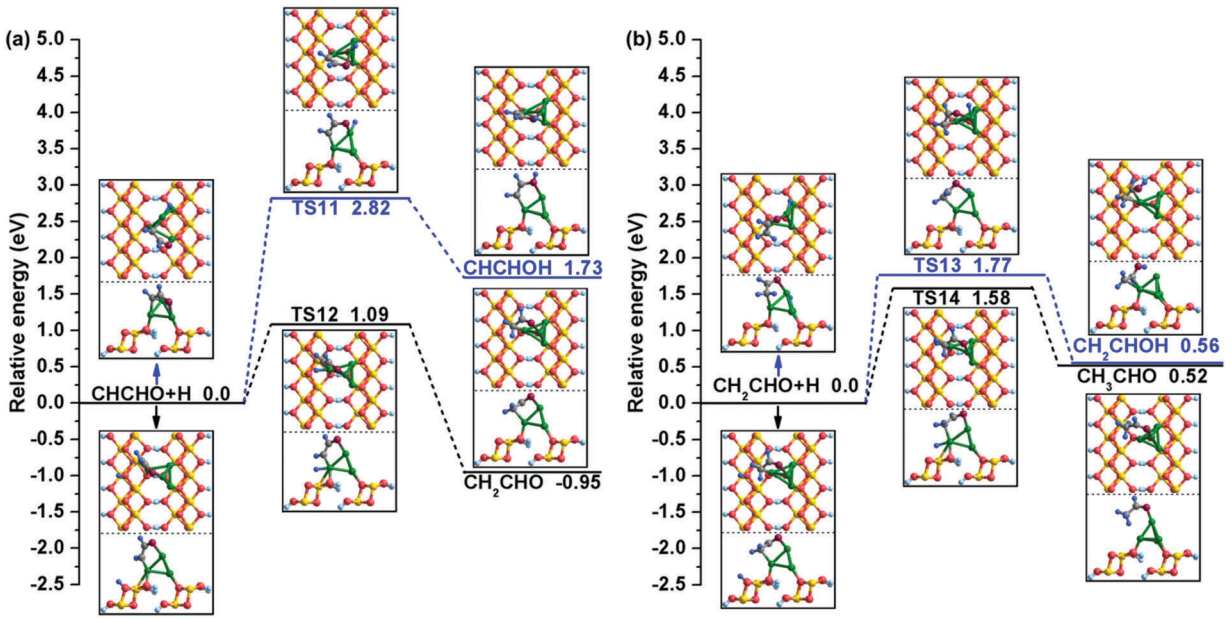

Fig. 6 The potential energy profiles for (a) CHCHO hydrogenation and (b) CH_2CHO hydrogenation with the structures of the initial states (ISs), transition states (TSs), and final states (FSs).

that CHO + CO → CH + CO_2 is more kinetically favorable on the γ-AlOOH(001) surface (E_a = 1.29 eV).[31]

In addition, the possible elementary reactions of CHO hydrogenation have been examined, and a detailed potential energy profile is presented in Fig. 4. When CHO and H species are co-adsorbed at the Cu/γ-AlOOH(001) surface, CHO occupies the Cu_1 and Cu_2 sites through its C and O atoms and the H binds at the bridge Cu_1–Cu_3 site. As displayed in Fig. 4, there are four possible products of CHO hydrogenation: CH + OH, CHOH, CH_2O and CH_2 + O. According to our calculation, the reaction CHO + H → CH + OH over the Cu/γ-AlOOH(001) surface is difficult; it must overcome a relatively high activation barrier of 3.00 eV with a reaction energy of −0.10 eV. The C–O bond distance increases to 2.559 Å from 1.278 Å in the co-adsorbed CHO and H. For the formation of CHOH, the distance between the O and H atoms decreases to 2.215 Å in TS4 from 3.416 Å in the initial state. In TS4, the dissociated H atom shifts to the surrounding CHO and then bonds with O atom. This elementary reaction has an activation barrier of 2.28 eV with a corresponding reaction energy of 1.00 eV. On the other hand, when the H atom moves to the C atom of CHO, the intermediate CH_2O is generated, with an activation barrier of

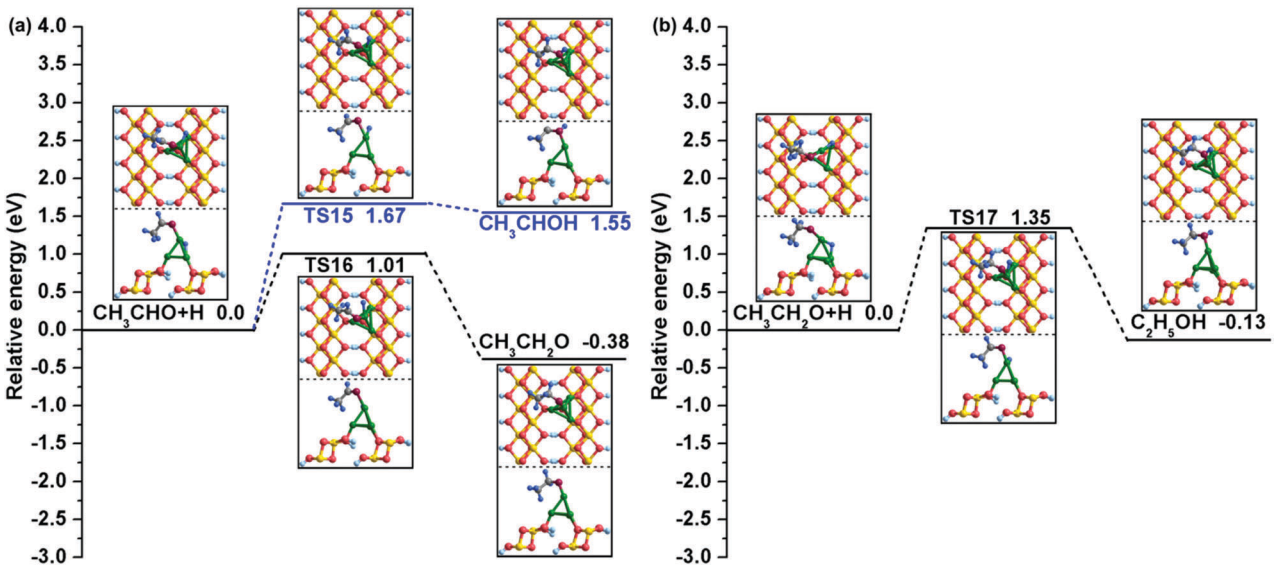

Fig. 7 The potential energy profiles for (a) CH_3CHO hydrogenation and (b) C_2H_5OH formation with the structures of the initial states (ISs), transition states (TSs), and final states (FSs).

Table 3 At a temperature of 563 K, the corresponding activation barriers (ΔG_a, eV) and reaction energies (ΔG, eV) involved in C–C formation, C–O cleavage, CH_2CHO hydrogenation and C_2H_5OH formation

Reaction	ΔG_a	ΔG
CHO + CHO → OHCCHO	1.09	−0.58
OHCCHO → CHCHO + O	1.46	0.36
$CH_2CHO + H \rightarrow CH_3CHO$	1.54	0.39
$CH_3CH_2O + H \rightarrow C_2H_5OH$	1.37	−0.11

1.94 eV and a reaction energy of 0.33 eV. For CH_2O formation, the distance between the C and H atoms decreases to 1.899 Å in TS5 from 3.655 Å. Simultaneously, the reaction of CHO hydrogenation and synchronous dissociation is considered here. In TS6, the distance between the C and H atoms decreases to 1.914 Å from 3.655 Å in the co-adsorbed CHO + H; this step must conquer a barrier of 1.47 eV, accompanied by a reaction energy of 0.52 eV.

All possible elementary reactions involving CHO have been carefully investigated in the above discussion. Comparing the corresponding activation barriers and reaction energies of these reactions, our calculation results confirm that CHO tends to generate the OHCCHO key intermediate among seven possible reactions; this has the lowest activation barrier of 1.07 eV and is thermodynamically advantageous, being exothermic by 0.73 eV. Actually, when OHCCHO is formed by means of CHO coupling, it is facile to assume that it is possible to generate ethylene glycol (HOH_2CCH_2OH) *via* successive hydrogenation of the OHCCHO precursor from the point of view of theoretical calculation; ethylene glycol is an important chemical that has a number of applications.[65] Therefore, as summarized in detail in Fig. S2–S4 (ESI†), we also considered the feasibility of HOH_2CCH_2OH formation on the Cu/γ-AlOOH(001) surface. Based on the thermodynamic and kinetic data determined in our DFT calculations, the optimal possible route of ethylene glycol formation *via* OHCCHO continuous hydrogenation is as follows: $OHCCHO + H \rightarrow OH_2CCHO + H \rightarrow HOH_2CCHO + H \rightarrow HOH_2CCH_2O + H \rightarrow HOH_2CCH_2OH$. Therefore, it is worthwhile to point out that HOH_2CCH_2OH is a possible product based on the OHCCHO key intermediate from a fundamental point of view.

3.2.3 C_2H_5OH formation. With respect to OHCCHO, C–O bond scission to produce CHCHO was examined. As shown in Fig. 5, the reactant OHCCHO bonds with the Cu_1 and Cu_3 sites through two O atoms, in which the distance between C_2 and O_2 atoms is measured to be 1.318 Å. Next, the O_2 atom breaks away from OHCCHO and shifts to the bridge Cu_1–Cu_3 site; the distance between the C_2 and O_2 atoms increases to 2.689 Å. The activation barrier and reaction energy of the CHCHO formation are 1.51 and 0.34 eV, respectively, which are in good agreement with our calculated activation free energy (1.46 eV) and reaction free energy (0.36 eV) shown in Table 3. Beginning with the C_2 species CHCHO in Fig. 6(a), there are two possible products of its hydrogenation: CHCHOH and CH_2CHO. For the formation of CHCHOH, the reactant CHCHO occupies the Cu_1, Cu_2 and Cu_4 sites and the H atom stays at the bridge Cu_1–Cu_3 site in the co-adsorbed CHCHO + H. Subsequently, the H atom gradually moves closer to CHCHO and finally bonds with the O atom to form CHCHOH. The distance between the O and H atoms decreases to 2.450 Å in TS11 from 4.461 Å, and the calculated activation barrier of this step is as high as 2.82 eV and is endothermic by 1.73 eV. In contrast to CHCHOH formation, for the reaction of CHCHO hydrogenation to CH_2CHO, the H atom is adsorbed on the Al_V site in the initial state. In TS12, the H atom migrates to the Cu_2 site while CHCHO remains at the bridge Cu_1–Cu_2 site, and the distance between the C_2 and H atoms decreases to 2.076 Å from 4.071 Å. In the FS, the H atom moves to the side of CHCHO and bonds with the C atom to generate CH_2CHO. Compared with the formation of CHCHOH, CH_2CHO formation must overcome a lower activation barrier of only 1.09 eV and is exothermic by 0.95 eV. It can be seen that CH_2CHO formation is more favorable *via* CHCHO hydrogenation both kinetically and thermodynamically.

As displayed in Fig. 6(b), there are also two possible products of continuous hydrogenation for CH_2CHO. One is $CH_2CHO + H \rightarrow CH_2CHOH$, which is endothermic by 0.56 eV and must conquer a relative high energy barrier of 1.77 eV. During this process, the isolated H atom gradually moves to the neighbour of CH_2CHO and finally bonds with the O atom to form CH_2CHOH. In TS13, the distance between the O and H atoms decreases to 1.840 Å from 3.223 Å. The other product is CH_3CHO on the Cu/γ-AlOOH(001) surface; this step starts from the bridge-adsorbed CH_2CHO and Al_V site-adsorbed H atoms, after which the single H atom moves to the Cu_2 site and finally forms the intermediate CH_3CHO with breakage of the C_2–Cu_2 bond and formation of the C_2–H bond. During this process, the distance between the C_2 and H atoms decreases to 2.536 Å in TS14 from 3.786 Å in the initial state; the calculated activation barrier is 1.58 eV with a reaction energy of 0.52 eV, which are similar to our calculated activation free energy (1.54 eV) and reaction free energy (0.39 eV) in Table 3. Based on the above DFT calculations, we can draw a conclusion that CH_2CHO hydrogenation tends to generate CH_3CHO, which has a lower activation barrier than CH_2CHOH formation over the Cu/γ-AlOOH(001) surface.

Similarly, our calculations suggested that there are also two possible reaction paths for CH_3CHO hydrogenation: one is bonding of the H atom to the O atom to form CH_3CHOH, and the other is C_1–H bond formation to generate CH_3CH_2O. As shown in Fig. 7(a), starting from the co-adsorbed $CH_3CHO + H$, the H atom residing at the bridge Cu_1–Cu_3 site travels to bond with the O atom of CH_3CHO to produce CH_3CHOH. This reaction must overcome a relatively high activation barrier of 1.67 eV with an assimilating energy of 1.55 eV. However, for CH_3CH_2O formation, the Cu/γ-AlOOH(001) surface presents better catalytic performance from both kinetic and thermodynamic perspectives. Our calculated activation barrier of this step is 1.01 eV and the reaction energy is −0.38 eV, and the distance between the C_1 and H atoms decreases to 2.559 Å in TS16 from 3.641 Å in the co-adsorbed CH_3CHO and H species. Eventually, the target product C_2H_5OH is generated by CH_3CH_2O hydrogenation at the α-C site. Similar to the CH_3CHO hydrogenation, as displayed in Fig. 7(b), the H adatom gradually moves close to the intermediate CH_3CH_2O and finally bonds with the O atom to form C_2H_5OH. Meanwhile, the distance

between the O and H atoms decreases to 1.730 Å in TS17 from 3.319 Å in the initial state with a corresponding activation barrier and reaction energy of 1.35 and −0.13 eV, respectively. As displayed in Table 3, our calculated activation free energy of C_2H_5OH formation *via* CH_3CH_2O hydrogenation is 1.37 eV, with a reaction free energy of −0.11 eV.

Based on the abovementioned calculations and from the point of view of the energy barriers, the optimal reaction pathway for ethanol synthesis from syngas on the Cu/γ-AlOOH(001) surface is CO + H → CHO, CHO + CHO → OHCCHO → CHCHO + O, CHCHO + 4H → CH_2CHO + 3H → CH_3CHO + 2H → CH_3CH_2O + H → C_2H_5OH. Moreover, the highest reaction barrier during the whole route is 1.58 eV, which is related to the formation of CH_3CHO. As presented in Fig. 8, through comprehensive study of the energies of each elementary reaction in the optimal pathway, we can divide this process into four stages:[66] the first stage is the initial CO activation to the formation of OHCCHO; the second stage includes the C–O bond cleavage and CH_3CHO formation; the third stage is CH_3CHO hydrogenation; and the last stage is the formation of C_2H_5OH. In this process, the rate-determining step is associated with the CHCHO hydrogenation in the second stage. However, it is worth noting that the C–C chain formation must conquer a barrier of only 1.07 eV *via* formyl coupling over the Cu/γ-AlOOH(001) surface; however, this differs to a large extent from the results over the γ-AlOOH(001) surface.[31] According to our previous study on the γ-AlOOH(001)[31] surface, the initial C–C chain is formed *via* CO insertion into CH, along with overcoming a 0.76 eV barrier, and is exothermic by 1.90 eV; the optimal route for syngas-to-ethanol conversion is CO → CHO → CH → CHCO → CHCOH → CHCHOH → CH_2CHOH → CH_2CH_2OH → C_2H_5OH, in which the formation of the CH species is the rate-determining step of the whole process, with an activation barrier of 1.21 eV. Therefore, the Cu component displays great influence upon the reaction mechanism of syngas conversion, especially impacting the mechanism of C–C bond formation, but does not show better CO activation ability and carbon chain growth. In contrast, the partial coverage of CuO_x species formed by the strong metal support interaction (SMSI) between the Cu component and the γ-AlOOH(001) surface strengthens the non-dissociative adsorption capacity of CO. This is because the adsorption energy of CO on Cu/γ-AlOOH(001) increases to 1.37 eV from 0.37 eV on the γ-AlOOH(001) surface,[31] which is even larger than the value on the pristine Cu surface (1.28 eV).[14] Furthermore, CO activation *via* direct dissociation or indirect H-assisted dissociation becomes more difficult than on γ-AlOOH(001) and Cu surfaces according to their activation barriers and reaction energies (For CO → C + O, ΔE = 3.71 eV on Cu/γ-AlOOH(001), E_a = 3.77 eV and ΔE = 2.77 eV on γ-AlOOH(001), E_a = 5.56 eV and ΔE = 1.54 eV on Cu(211); for CO + H → CHO, E_a = 1.30 eV and ΔE =0.55 eV on Cu/γ-AlOOH(001), E_a = 1.04 eV and ΔE = −0.31 eV on γ-AlOOH(001), E_a = 1.12 eV and ΔE = 0.74 eV on Cu(211)).[14,31] However, compared with the γ-AlOOH(001) surface[31] (E_a = 0.76 eV and ΔE = −1.90 eV) for the carbon chain growth, the Cu/γ-AlOOH(001) surface does not display an advantage (E_a = 1.00 eV and ΔE = −0.73 eV) but is still more favorable than the Cu(211) surface (E_a = 1.46 eV and ΔE = 0.03 eV).[14] Hence, from the comparison analysis, we confirmed that the Al component plays a pivotal role in the carbon chain growth.

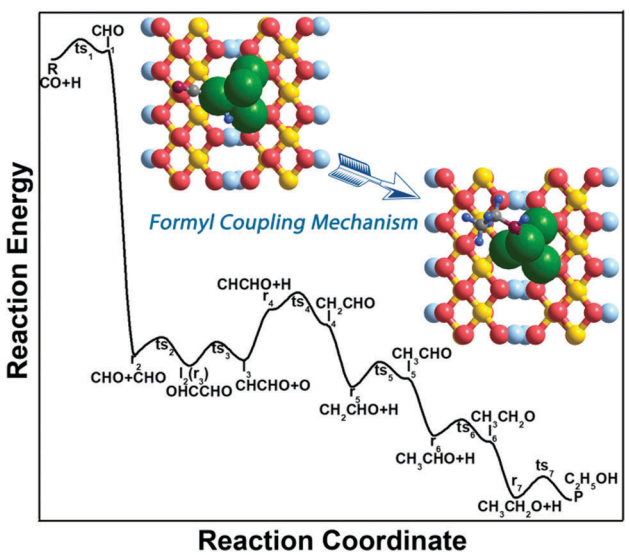

Fig. 8 The optimal reaction pathway diagram for ethanol formation from syngas over the Cu/γ-AlOOH(001) surface.

3.3 Bader charge analyses

In contrast to the γ-AlOOH(001) surface,[31] the initial C–C bond formation during the process of syngas-to-ethanol conversion over the Cu/γ-AlOOH(001) surface occurs through two CHO species coupling with a relatively high activation barrier. To obtain an in-depth understanding of the mechanism of C–C chain formation, Bader charge analysis was employed in this section. Firstly, the Bader charges of the clean Cu/γ-AlOOH(001) surface were calculated; as shown in Fig. 9(a), the charges of the Cu_1, Cu_2, Cu_3 and Cu_4 sites are +0.03 $|e|$, +0.34 $|e|$, +0.38 $|e|$ and +0.38 $|e|$, respectively. It has been stated that the Cu component which is close to the γ-AlOOH(001) surface transfers more electrons to the surface *via* the SMSI effect. It is well known that SMSI can offer a route to control the structural properties of the γ-AlOOH(001)-supported Cu particle and, hence, its reactivity and stability, resulting in a marked effect on the catalytic performance. Moreover, SMSI is often accompanied with electron transfer between the metal and support, which is defined as electronic metal-support interaction (EMSI).[67,68] Exactly, as shown in Fig. 9(a), the γ-AlOOH(001) surface transfers an electron with the Cu component, as shown by comparing the charges of the O sites with the pristine γ-AlOOH(001) surface.[31] Eventually, the formed CuO_x species *via* the SMSI between the Cu and Al components affects the adsorption strength of the correlated species; this results in a different reaction route.

When the CHO species adsorbs at the surface, as shown in Fig. 9(b), the Bader charge of the Cu_1 site increases to +0.17 $|e|$ because it loses electrons to CHO; the Cu_2 site slightly increases to +0.36 $|e|$, the Cu_3 site decreases to +0.28 $|e|$ and the Cu_4 site decreases to +0.31 $|e|$. Meanwhile, CHO occupies the bridge Cu_1–Cu_2 site *via* the O and C atoms, and the net charge of

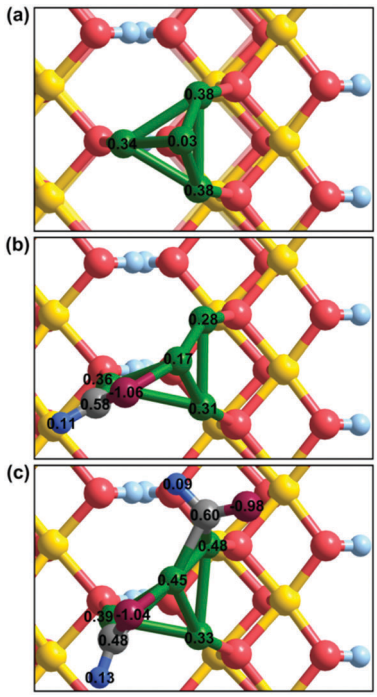

Fig. 9 Calculated Bader charges: (a) the Cu/γ-AlOOH(001) surface; (b) CHO on the Cu/γ-AlOOH(001) surface; (c) CHO + CHO on the Cu/γ-AlOOH(001) surface.

adsorbed CHO is −0.37 |*e*|. Actually, the charges of these O sites on the γ-AlOOH(001) surface, which directly interact with the Cu_2, Cu_3 and Cu_4 sites of the Cu component, increase by only 0.02 to 0.03 |*e*|. It can be seen that the interaction of the Cu component and the γ-AlOOH(001) surface does not change remarkably after adsorbing CHO. Regarding the initial C–C chain formation in Fig. 9(c), the net charges carried by the reactants CHO + CHO, which reside in the bridge Cu_1–Cu_2 site and the bridge Cu_1–Cu_3 site, are −0.43 |*e*| and −0.29 |*e*|, respectively. Meanwhile, the charges of the Cu_1 and Cu_3 sites increase to +0.45 |*e*| and +0.48 |*e*|, while the charges of the Cu_2 and Cu_4 sites are almost unchanged. Obviously, upon adding a second adsorbed CHO, the electrostatic interaction between the reactants and adsorption sites becomes stronger, which also results in enhancement of the adsorption stability of the reactants. However, the electron transfer between Cu and γ-AlOOH(001) is still similar to those in Fig. 9(a) and (b). Moreover, the charges of the C atoms in the CHO species are +0.48 |*e*| and +0.60 |*e*|, respectively. Therefore, comparing with the known nucleophilic attack mechanism *via* CO insertion into the neighboring CH_x species, the formyl coupling mechanism for carbon chain growth must overcome a relatively high activation barrier over the Cu/γ-AlOOH(001) surface.

3.4 Rate constant analyses

With the aim of exploring the effects of the reaction temperature on ethanol synthesis from syngas, the rate constants of some key elementary reactions at different temperatures are calculated in this section. It has been reported that the productivity of $C_{2+}OH$ is negligible if the reaction temperature is below 533 K; in the temperature range from 543 K to 583 K, Cu-based catalysts show good catalytic activity[12,69,70] Additionally, combining previous discoveries[12,14] with our calculation results showing the optimal reaction pathway for ethanol synthesis on the Cu/γ-AlOOH(001) surface, we confirmed that C–C bond formation, C–O cleavage, CH_3CHO and C_2H_5OH formation are the key steps in the whole process. Therefore, the rate constants of the above four elementary reactions in the temperature range of 543 to 583 K were investigated, and the corresponding rate constants are listed in Table 4. The corresponding values from 543 K to 583 K are 7.97×10^2 to 4.12×10^3, 3.35×10^{-1} to 2.87, 6.12×10^{-2} to 5.38×10^{-1}, and 2.30 to 1.45×10^1 s^{-1}, respectively. It can be clearly seen that the rate constants *k* of these steps increase stepwise with increasing temperature on the Cu/γ-AlOOH(001) surface, which indicates a positive correlation between the reaction temperature and the rate constants. Furthermore, at the same temperature, the order of the rate constants of the above four key reactions is *k*(C–C bond formation) > *k*(C_2H_5OH formation) > *k*(C–O bond cleavage) > *k*(CH_3CHO formation); this order is consistent with that of the reaction barriers of these elementary reactions. Especially, C–C bond formation *via* formyl coupling possesses the maximum rate constant, suggesting that carbon chain growth is also favorable on the Cu/γ-AlOOH(001) model.

4 Conclusions

In the present study, the reaction mechanism of syngas conversion into ethanol on the Cu/γ-AlOOH(001) surface has been investigated systematically using periodic DFT calculations at the molecular level. The adsorption energies of the involved species as well as the activation barriers and reaction energies of the possible elementary reactions during the process of syngas-to-ethanol conversion were calculated. Guided by our detailed DFT results, the optimal route of syngas conversion into ethanol over the Cu/γ-AlOOH(001) surface is as follows: CO + H → CHO, CHO + CHO → OHCCHO → CHCHO + O,

Table 4 Rate constants *k* (s^{-1}) of C–C formation, C–O cleavage, CH_2CHO hydrogenation and C_2H_5OH formation involved in the process of ethanol synthesis

	Rate constant *k* (s^{-1})				
Elementary reaction	543 K	553 K	563 K	573 K	583 K
CHO + CHO → OHCCHO	7.97×10^2	1.22×10^3	1.86×10^3	2.79×10^3	4.12×10^3
OHCCHO → CHCHO + O	3.35×10^{-1}	5.90×10^{-1}	1.02	1.73	2.87
$CH_2CHO + H \rightarrow CH_3CHO$	6.12×10^{-2}	1.09×10^{-1}	1.89×10^{-1}	3.21×10^{-1}	5.38×10^{-1}
$CH_3CH_2O + H \rightarrow C_2H_5OH$	2.30	3.72	5.95	9.38	1.45×10^1

$CHCHO + 4H \rightarrow CH_2CHO + 3H \rightarrow CH_3CHO + 2H \rightarrow CH_3CH_2O + H \rightarrow C_2H_5OH$, in which CH_3CHO formation needs to overcome the highest activation barrier (1.58 eV) in the whole pathway. Different from the γ-AlOOH(001) surface,[31] the initial C–C chain formation over the Cu/γ-AlOOH(001) surface occurs *via* formyl coupling to form the OHCCHO key intermediate; this process is exothermic by 0.73 eV and must conquer a corresponding activation barrier of 1.07 eV. Moreover, Bader charge analyses showed a strong electrostatic interaction between the CHO intermediate and the formed CuO_x species; the electrostatic repulsive interaction of CHO species is relative detrimental to carbon chain growth *via* CHO coupling over the Cu/γ-AlOOH(001) surface, comparing with the formation way *via* CO insertion into CH over the γ-AlOOH(001) surface.[31] Taking temperature effects into account, we found it shows a positive correlation with the rate constants, especially for C–C chain formation; the corresponding rate constants increase to $4.12 \times 10^3\ s^{-1}$ from $7.97 \times 10^2\ s^{-1}$ in the range of 543 to 583 K. In summary, the addition of the Cu component exhibits great influence on the mechanism of syngas conversion over the γ-AlOOH(001) surface, especially on C–C bond formation. However, on the Cu/γ-AlOOH(001) surface, the formation of the OHCCHO intermediate provides the possibility to form other C_2 dioxides during syngas conversion.

Conflicts of interest

There are no conflicts to declare.

Acknowledgements

The authors acknowledge financial support from the Key Projects of the National Natural Science Foundation of China (No. 21336006), the National Natural Science Younger Foundation of China (No. 21703151), the National Natural Science Foundation of China (No. 21776195), the Scientific and Technological Innovation Programs of Higher Education Institutions in Shanxi (STIP, No. 201802052), the Graduate Education Innovation Program of Shanxi Province (No. 2018BY049), the Natural Science Younger Foundation of Shanxi Province (No. 201601D202017), and the Natural Science Foundation of Shanxi Province (No. 201601D011021).

References

1 X. Pan, Z. Fan, W. Chen, Y. Ding, H. Luo and X. Bao, *Nat. Mater.*, 2007, **6**, 507–511.
2 A. M. Henstra, J. Sipma, A. Rinzema and A. J. M. Stams, *Curr. Opin. Biotechnol.*, 2007, **18**, 200–206.
3 C. S. Song, *Catal. Today*, 2006, **115**, 2–32.
4 V. M. Thomas and A. Kwong, *Energy Policy*, 2001, **29**, 1133–1143.
5 L. Siwale, L. Kristóf, T. Adam, A. Bereczky, A. Penninger, M. Mbarawa and K. Andrei, *J. Power Energy*, 2013, **1**, 77–83.
6 B. O. Palsson, S. Faith-Afshar, D. F. Rudd and E. N. Lightfoot, *Science*, 1981, **213**, 513–517.
7 T. K. Ng, R. M. Busche, C. C. Mcdonald and R. W. F. Hardy, *Science*, 1983, **219**, 733–740.
8 C. Lamy, S. Rousseau, E. M. Belgsir, C. Coutanceau and J. M. Léger, *Electrochim. Acta*, 2004, **49**, 3901–3908.
9 S. Velu, N. Satoh, C. S. Gopinath and K. Suzuki, *Catal. Lett.*, 2002, **82**, 145–152.
10 D. A. Deluga, J. R. Salge, L. D. Schmidt and X. E. Verykios, *Science*, 2004, **303**, 993–997.
11 H. T. Luk, C. Mondelli, D. C. Ferré, J. A. Stewart and J. Pérez-Ramírez, *Chem. Soc. Rev.*, 2017, **46**, 1358–1426.
12 J. J. Spivey and A. Egbebi, *Chem. Soc. Rev.*, 2007, **36**, 1514–1528.
13 V. Subramani and S. K. Gangwal, *Energy Fuels*, 2008, **22**, 814–839.
14 R. G. Zhang, G. R. Wang and B. J. Wang, *J. Catal.*, 2013, **305**, 238–255.
15 Z. J. Zuo, L. Wang, L. M. Yu, P. D. Han and W. Huang, *J. Phys. Chem. C*, 2014, **118**, 12890–12898.
16 R. G. Zhang, G. R. Wang, B. J. Wang and L. X. Ling, *J. Phys. Chem. C*, 2014, **118**, 5243–5254.
17 G. R. Wang, R. G. Zhang and B. J. Wang, *Appl. Catal., A*, 2013, **466**, 77–89.
18 J. Sun, Q. X. Cai, Y. Wan, S. L. Wan, L. Wang, J. D. Lin, D. H. Mei and Y. Wang, *ACS Catal.*, 2016, **6**, 5771–5785.
19 M. Gupta, M. L. Smith and J. J. Spivey, *ACS Catal.*, 2011, **1**, 641–656.
20 S. Kattel, P. J. Ramírez, J. G. Chen, J. A. Rodriguez and P. Liu, *Science*, 2017, **355**, 1296–1299.
21 W. Huang, L. M. Yu, W. H. Li and Z. L. Ma, *Front. Chem. Eng. China*, 2010, **4**, 472–475.
22 S. R. Yu, Y. E. Chen, S. S. Gao, X. D. Wang and W. Huang, *Energy Sources, Part A*, 2013, **35**, 955–961.
23 Y. J. Liu, Z. J. Zuo, C. Li and X. Deng, *Appl. Surf. Sci.*, 2015, **356**, 124–127.
24 Y. J. Liu, C. B. Liu, X. Deng and W. Huang, A study on deactivation of Cu-Zn-Al catalyst for higher alcohols synthesis, *RSC Adv.*, 2015, **5**, 99023–99027.
25 X. Deng, Y. J. Liu and W. Huang, Higher alcohols synthesis from syngas over lanthanum-promoted CuZnAl catalyst, *J. Energy Chem.*, 2018, **27**, 319–325.
26 Z. H. Gao, W. Huang, L. H. Yin, L. F. Hao and K. C. Xie, *Catal. Lett.*, 2009, **127**, 354–359.
27 R. R. Wei, Z. H. Gao, S. H. Hao and W. Huang, *Chin. J. Chem. Eng.*, 2015, **66**, 2112–2117.
28 Y. M. Han, Z. H. Gao and W. Huang, *Chin. J. Chem.*, 2017, **38**, 823–829.
29 L. L. Li, H. H. Tian, Y. M. Han, Y. Liu and Z. H. Gao, *J. Fuel Chem. Technol.*, 2016, **44**, 830–836.
30 L. Zhang, B. Bai, H. Bai, W. Huang, Z. H. Gao, Z. J. Zuo and Y. K. Lv, *Phys. Chem. Chem. Phys.*, 2017, **19**, 19300–19307.
31 B. Bai, H. Bai, L. Zhang and W. Huang, *Appl. Surf. Sci.*, 2018, **455**, 123–131.
32 D. Chiche, M. Digne, R. Revel and J. P. Jolivet, *J. Phys. Chem. C*, 2008, **112**, 8524–8533.
33 M. Nguefack, A. F. Popa, S. Rossignol and C. Kappenstein, *Phys. Chem. Chem. Phys.*, 2003, **5**, 4279–4289.
34 Y. Noel, R. Demichelis, F. Pascale, P. Ugliengo, R. Orlando and R. Dovesi, *Phys. Chem. Miner.*, 2009, **36**, 47–59.

35 P. Alphonse and M. Courty, *Thermochim. Acta*, 2005, **425**, 75–89.
36 J. R. Li, R. G. Zhang and B. J. Wang, *Appl. Surf. Sci.*, 2013, **270**, 728–736.
37 Y. X. Pan, C. J. Liu and Q. F. Ge, *J. Catal.*, 2010, **272**, 227–234.
38 D. Lomot and Z. Karpinski, *Catal. Lett.*, 2000, **69**, 133–138.
39 J. A. Rodriguez, J. Evans, J. Graciani, J. B. Park, P. Liu, J. Hrbek and J. F. Sanz, *J. Phys. Chem. C*, 2009, **113**, 7364–7370.
40 R. G. Zhang, M. Peng, T. Duan and B. J. Wang, *Appl. Surf. Sci.*, 2017, **407**, 282–296.
41 D. Chiche, M. Digne, R. Revel and J. P. Jolivet, *J. Phys. Chem. C*, 2008, **112**, 8524–8533.
42 P. Raybaud, M. Digne, R. Iftimie, W. Wellens, P. Euzen and H. Toulhoat, *J. Catal.*, 2001, **201**, 236–246.
43 G. Kresse and J. Furthmüller, *Phys. Rev. B: Condens. Matter Mater. Phys.*, 1996, **54**, 11169–11186.
44 G. Kresse and J. Furthmüller, *Comput. Mater. Sci.*, 1996, **6**, 15–50.
45 J. P. Perdew, K. Burke and M. Ernzerhof, *Phys. Rev. Lett.*, 1996, **77**, 3865–3868.
46 P. E. Blöchl, *Phys. Rev. B: Condens. Matter Mater. Phys.*, 1994, **50**, 17953–17979.
47 G. Kresse and D. Joubert, *Phys. Rev. B: Condens. Matter Mater. Phys.*, 1999, **59**, 1758–1775.
48 S. N. Steinmann and C. Corminboeuf, *J. Chem. Phys.*, 2011, **134**, 044117.
49 S. N. Steinmann and C. Corminboeuf, *J. Chem. Theory Comput.*, 2011, **7**, 3567–3577.
50 H. J. Monkhorst and J. D. Pack, *Phys. Rev. B: Solid State*, 1976, **13**, 5188–5192.
51 J. Greeley and M. Mavrikakis, *Surf. Sci.*, 2003, **540**, 215–229.
52 X. M. Cao, R. Burch, C. Hardacre and P. Hu, *Catal. Today*, 2011, **165**, 71–79.
53 Y. J. Liu, C. B. Liu, C. Li and W. Huang, *Catal. Commun.*, 2016, **76**, 29–32.
54 H. Eyring, *Chem. Rev.*, 1935, **17**, 65–77.
55 D. G. Truhlar, B. C. Garrett and S. J. Klippenstein, *J. Phys. Chem.*, 1996, **100**, 12771–12800.
56 Y. M. Choi and P. Liu, *J. Am. Chem. Soc.*, 2009, **131**, 13054–13061.
57 Y. H. Zhao, M. M. Yang, D. Sun, H. Y. Su, K. Sun, X. Ma, X. Bao and W. X. Li, *J. Phys. Chem. C*, 2011, **115**, 18247–18256.
58 C. T. Campbell, L. Arnadottir and J. R. V. Sellers, *Z. Phys. Chem.*, 2013, **227**, 1435–1454.
59 A. Deluzarche, J. P. Hindermann, R. Kieffer, R. Breault and A. Kiennemann, *J. Phys. Chem.*, 1984, **88**, 4993–4995.
60 C. Diagne, H. Idriss, J. P. Hindermann and A. Kiennemann, *Appl. Catal.*, 1989, **51**, 165–180.
61 M. Xu and E. Iglesia, *J. Catal.*, 1999, **188**, 125–131.
62 D. J. Elliott and F. Pennella, *J. Catal.*, 1988, **114**, 90–99.
63 A. J. Medford, J. Sehested, J. Rossmeisl, I. Chorkendorff, F. Studt, J. K. Nørskov and P. G. Moses, *J. Catal.*, 2014, **309**, 397–407.
64 J. Nakamura, I. Nakamura, T. Uchijima, Y. Kanai, T. Watanabe, M. Saito and T. Fujitani, *J. Catal.*, 1996, **160**, 65–75.
65 H. Yue, Y. Zhao, X. Ma and J. Gong, *Chem. Soc. Rev.*, 2012, **41**, 4218–4244.
66 J. R. Murdoch, *J. Chem. Educ.*, 1981, **58**, 32–36.
67 Q. Fu and T. Wagner, *Surf. Sci. Rep.*, 2007, **62**, 431–498.
68 C. T. Campbell, *Nat. Chem.*, 2012, **4**, 597–598.
69 I. Boz, M. Sahibzada and I. S. Metcalfe, *Ind. Eng. Chem. Res.*, 1994, **33**, 2021–2028.
70 N. Kapur, J. Hyun, B. Shan, J. B. Nicholas and K. Cho, *J. Phys. Chem. C*, 2010, **114**, 10171–10182.